Molecular dynamics simulation on devitrification: Isothermal devitrification and thermodynamics of PbF 2 glasses

Maurcio A. P. Silva, José Pedro Rino, André Monteil, Sidney J. L. Ribeiro, and Younès Messaddeq

Citation: The Journal of Chemical Physics **121**, 7413 (2004); doi: 10.1063/1.1796252
View online: http://dx.doi.org/10.1063/1.1796252
View Table of Contents: http://scitation.aip.org/content/aip/journal/jcp/121/15?ver=pdfcov
Published by the AIP Publishing

Molecular dynamics simulation on devitrification: Isothermal devitrification and thermodynamics of PbF_2 glasses

Maurício A. P. Silva[a] and José Pedro Rino
Departamento de Física, Universidade Federal de São Carlos, Via Washington Luiz km235, 13565-905 São Carlos, São Paulo, Brazil

André Monteil
POMA UMR CNRS 6136, Université d'Angers, 2 boulevard Lavoisier, 49045 Angers, France

Sidney J. L. Ribeiro and Younès Messaddeq
Instituto de Química-UNESP, CP 355, 14801-970 Araraquara, São Paulo, Brazil

(Received 13 April 2004; accepted 29 July 2004)

The vitrification and devitrification features of lead fluoride are investigated by means of molecular dynamic simulations. The influence of heating rate on the devitrification temperature as well as the dependence of the glass properties on its thermal history, i.e., the cooling rate employed, is identified. As expected, different glasses are obtained when the cooling rates differ. Diffusion coefficient analysis during heating of glass and crystal, indicates that the presence of defects on the glassy matrix favors the transition processes from the ionic to a superionic state, with high mobility of fluorine atoms, responsible for the high anionic conduction of lead fluoride. Nonisothermal and isothermal devitrification processes are simulated in glasses obtained at different cooling rates and structural organizations occurring during the heat treatments are clearly observed. When a fast cooling rate is employed during the glass formation, the devitrification of a single crystal (limited by the cell dimensions) is observed, while the glass obtained with slower cooling rate, allowing relaxations and organization of various regions on the glass bulk during the cooling process, devitrifies in more than one crystalline plane. © *2004 American Institute of Physics.*
[DOI: 10.1063/1.1796252]

I. INTRODUCTION

The control of glass crystallization has been one of the most exciting challenges to glass researchers. The interest in the first steps of crystallization has grown with the development of glass-ceramic technologies, since control of devitrification requires a controlled nucleation, with well determined concentration and kind of nuclei.

With the advent of computational sciences, glasses have been studied by molecular modeling methods, such as molecular dynamics (MD), in its structure and structure-related properties, such as ion conduction,[1] luminescence,[2] vibrational spectra,[3] etc. Despite the possibilities raised with molecular modeling of structural determination of glasses, little work has been reported of molecular dynamic simulations of devitrification, including investigations of the nucleation and crystal growth processes.

Recently, MD simulations of the crystallization of a pure lead fluoride (PbF_2) glass have been reported.[4] Using molecular dynamics methods, the dynamic properties during vitrification and crystallization from the melt and glass crystallization using nonisothermal procedures have been simulated. Heating the PbF_2 glass results in the formation of a well-ordered structure with interionic Pb-Pb distances in total agreement with the expected face centred cubic PbF_2 structure. The cooling rate employed during simulations of glass formation was 100 K/ps, and the heating rate for simulations of devitrification, 1.5 K/ps. With these thermal characteristics, glass crystallization occurs at about 650 K.[4]

The basic objective of this paper is to explore the temperature dependences of the dynamic properties during PbF_2 glass formation and crystallization, by molecular dynamic simulations. For the simulations, the interionic pair potentials used were those proposed by Walker, Dixon, and Gillan,[5] which was successfully employed in the devitrification studies of PbF_2 in our previous work.[4] The results are presented in the following two sections: in Sec. II, the influence of the heating rate q on the nonisothermal crystallization of the glass is investigated and, in Sec. III, we describe the dependence of dynamic properties on the thermal history of the glasses, with two PbF_2 glasses obtained from different cooling rates ($q=-100$ and -10 K/ps) considered. Sections IV and V are devoted to discussions and conclusions.

II. INFLUENCE OF THE HEATING RATE ON THE DEVITRIFICATION TEMPERATURE

At first, a PbF_2 glass, at 50 K, with 2592 particles, was obtained, as described elsewhere,[4] by cooling from the melt, at 3000 K, with a cooling rate of $q=-100$ K/ps. From this glass three different constant-heating procedures were performed. Figure 1 shows the variation of the total energy of the system, as a function of the temperature, during the simulation of glass heating at $q_1=+1$ K/ps (black circles), $q_2=+3$ K/ps (triangles), and $q_3=+5$ Kps (squares). The

[a]Electronic mail: mauricio@df.ufscar.br

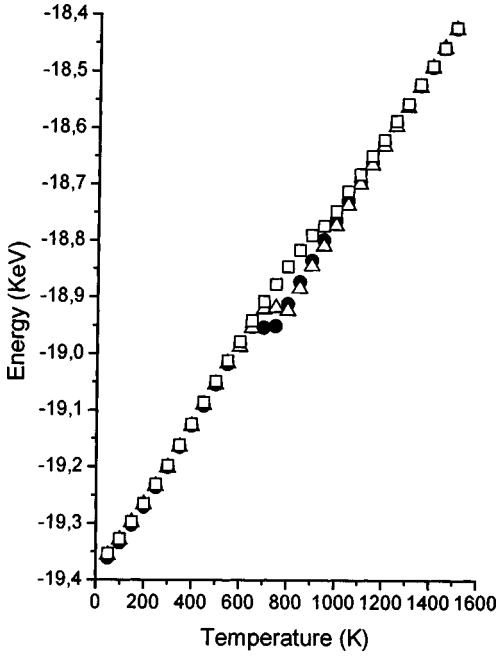

FIG. 1. Internal energy variation with temperature during heating of the glass at three different rates: $q=+1$ K/ps (black circles), $q=+3$ K/ps (triangles) and $q=+5$ K/ps (squares).

changes from linearity are related to the devitrification (exothermic transition). The increase of the devitrification temperature with increasing heating rate is clearly observed. Moreover, the temperature range in which devitrification occurs is larger when faster heating rates are employed.

III. INFLUENCES OF THE THERMAL HISTORY ON GLASSES

During a cooling process from the melt, the temperature range in which the glass transition occurs is strongly dependent on the cooling rate employed: the slower the cooling rate, the lower will be the glass transition temperature. A frequently observed experimental consequence of this behavior is that a glass prepared with a faster cooling rate is expected to have higher T_g and T_c values than those prepared with slower cooling processes.

To analyze these properties of glass formation and crystallization with respect to the cooling rate, several MD simulations have been done. Starting from a liquid at 3000 K, two different glasses at a final temperature of 50 K were prepared using two different cooling rates: $q_1=-10$ K/ps and $q_2=-100$ K/ps. The glasses obtained through these procedures will hereafter be called g-10 and g-100, respectively, relating the labels with the thermal history (cooling rates) of the glasses.

The plot of total energy as a function of temperature for the two cooling regimes is shown in Fig. 2 (left y axis). No exothermic transition is observed during this process (which would indicate a crystallization from the melt) and the pair distribution functions $g(r)$ shown in Fig. 3, display amorphouslike profiles, although some structural evolution is clearly observed in Pb-F and F-F pairs in both g-10 and g-100, and also in Pb-Pb pairs in g-10.

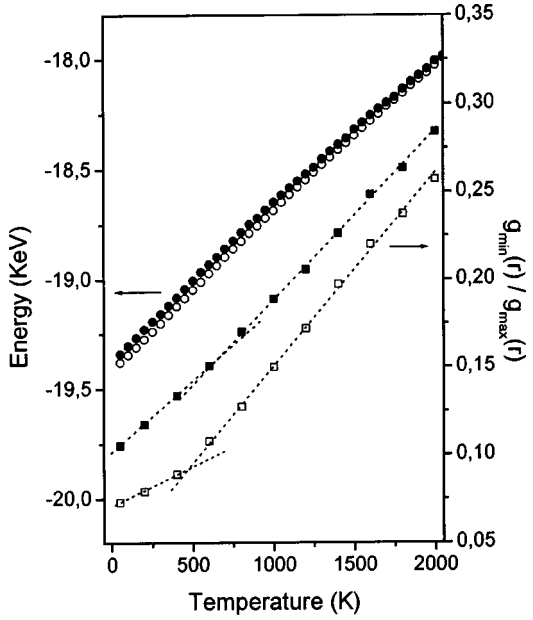

FIG. 2. Total energy (left y axis, circles) and $g_{\min}(r)/g_{\max}(r)$ (right y axis, squares) vs temperature during the two cooling regimes. Open symbols g-10, closed symbols g-100.

The glass transition temperature can be evaluated through the relation between the first minimum and the first maximum on the $g(r)$ curves.[6] The ratio $g_{\min}(r)/g_{\max}(r)$ allows us to determine whether the system is liquid or solid, and a plot of $g_{\min}(r)/g_{\max}(r)$ versus temperature for a glass indicates the glass transition temperature (considering the

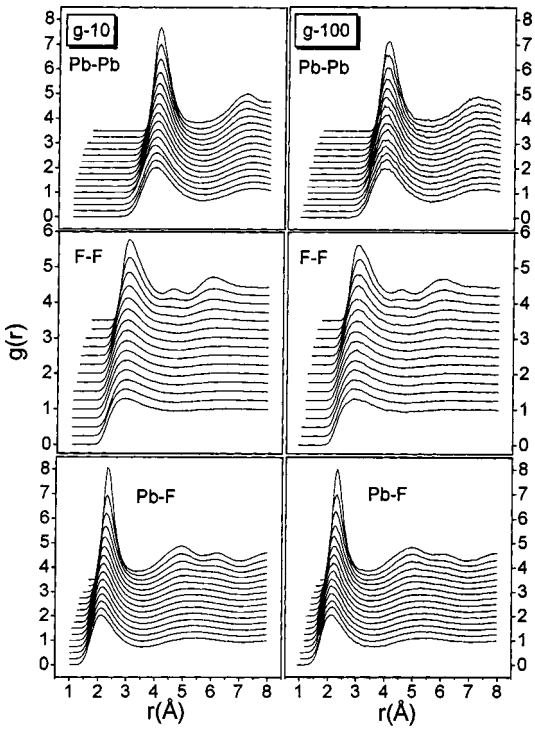

FIG. 3. Pair distribution functions $g(r)$ during the two cooling regimes, collected from 3000 to 200 K, each 200 K. For each atomic pair, the $g(r)$ curves for the different temperatures were y shifted for a better visualization: from bottom to top: 3000, 2800, 2600, 2400, 2200, 2000, 1800, 1600, 1400, 1200, 1000, 800, 600, 400, and 200 K.

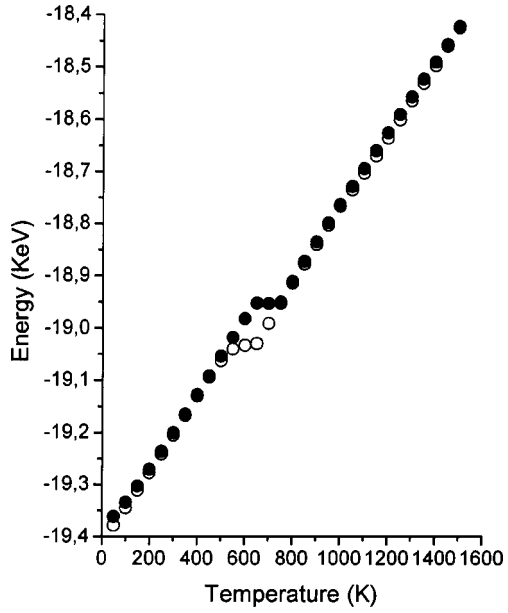

FIG. 4. Changes in the total energies with temperature, during the heating process of both glasses. Heating rate $q=+1$ K/ps. Open circles g-10, closed circles g-100.

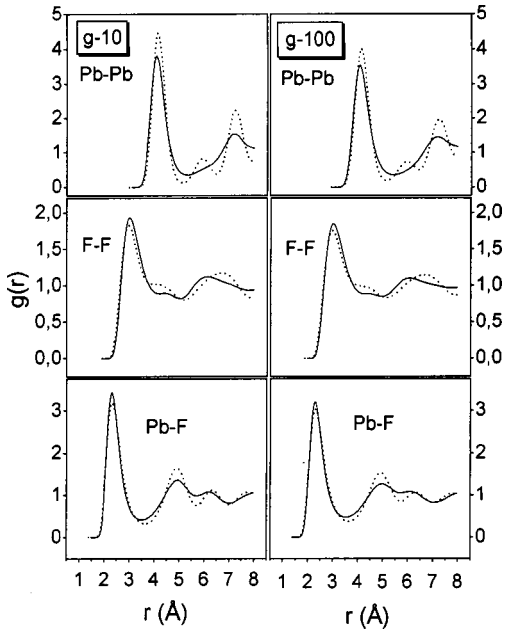

FIG. 5. Pair distribution functions, $g(r)$, during heating of both glasses at $q=+1$ K/ps. For g-10, line denotes the $g(r)$ obtained at 500 K (before devitrification) and dots at 700 K (after devitrification). Similarly, for g-100, line denotes the $g(r)$ obtained at 600 K and dots the $g(r)$ at 800 K, before and after devitrification.

simple assumption that T_g is the temperature at which the undercooled melt reaches the viscosity of a solid, $\sim 10^{13}$ Poise). This has been made for the two vitrification procedures, considering the Pb-Pb pair distribution functions, and the respective plots of $g_{\min}(r)/g_{\max}(r)$ versus temperature are shown on the right y axis of Fig. 2. Two linear regions are observed, and the temperature at which the slope changes indicates the glass transition temperature: it occurs at about 480 K for g-10 and 630 K for g-100.

It is clear from Figs. 2 and 3 that different cooling rates result in different glasses: g-10 has lower T_g and internal energy values than g-100, and structural organizations are also more pronounced in g-10. Naturally it is expected that these glasses, as quenched, present different devitrification features.

Simulations of nonisothermal devitrification were performed, as described elsewhere,[4] by heating at a constant rate of $q=+1$ K/ps, for both glasses. The changes in the total energies with temperature, during the heating process, are displayed in Fig. 4. Exothermal transitions are observed around 550 K for g-10 glass and around 650 K for g-100 glass. Devitrification is confirmed through $g(r)$ analysis, as shown in Fig. 5. The different devitrification temperatures observed for g-10 and g-100 glasses are expected when dissimilar thermal history is present.[7]

The approximate diffusion coefficients D of lead and fluorine atoms in the glasses were recorded during the constant heating studies. Figure 6 shows the variation in atomic diffusion in glasses g-10 and g-100, and the crystalline β-PbF_2 with temperature. The diffusion coefficients of fluorine atoms on both glasses present a similar evolution with temperature. The anionic diffusion coefficients in these glasses are larger than those observed in the corresponding crystal. On the other hand, lead atoms present dissimilar diffusion characteristics in the glasses and the crystal. While in the crystal the diffusion coefficient of the cations presents no discernible changes before fusion,[4] in the glasses it reaches a maximum at 600 K in g-10 and 700 K in g-100 glass.

Figure 7 displays how total energy changes with time, during the constant glass-heating simulations. Data for g-100 were energy-shifted by +100 eV, for a better visualization. For the heating rate of 1 K/ps adopted here, the temperature is increased in steps of 50 K in a time interval of 50 ps. It is clear that, as the simulation proceeds, the ''nonisothermal''

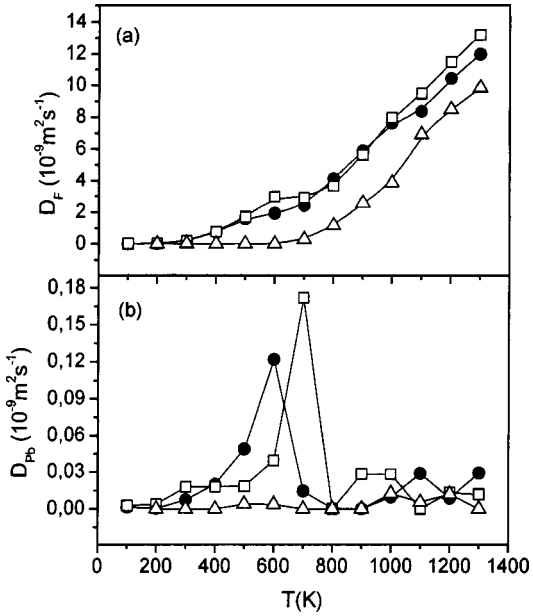

FIG. 6. Changes in the diffusion coefficient of fluorine (a) and lead (b) atoms in glasses g-10 (black circles) and g-100 (squares) and the crystalline β-PbF_2 (triangles) with rising temperature.

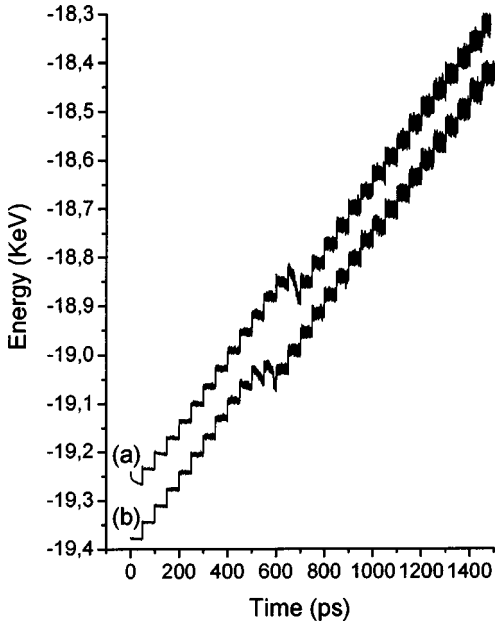

FIG. 7. Total energy changes with time, during constant glass-heating procedures. (a) g-100; (b) g-10. Data for g-100 were energy-shifted on +100 eV, for a better visualization.

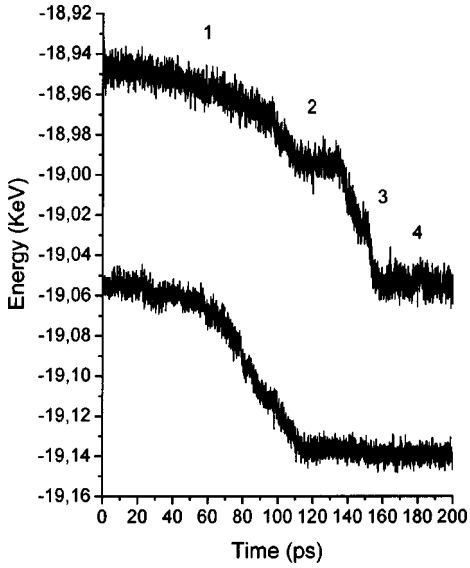

FIG. 8. Variation of the total energy with time during isothermal devitrification of both glasses. Bottom g-10, $T=500$ K; top g-100, $T=650$ K. See text for explanations on labels 1–4.

heat treatment consists of a sequence of isothermal steps 50 ps apart. Each energy plateau is related to the respective simulation temperature, the first plateau at 50 K, the second at 100 K and so on. We detect the devitrification by the stabilization processes occurring at various energy plateau, for both g-10 and g-100. This nonisothermal treatment led thus to devitrification processes going on over an extended range of temperature, depending on the heating rate, rather than at a fixed temperature value. Note that while the g-10 system starts to crystallize around 500 K, the g-100 will show this kind of behavior only around 650 K. Another important point to be noted in Fig. 7 is in the beginning of the MD run. During the first 50 ps evolution time at 50 K, the g-10 system energy displays an oscillation around a mean value, while g-100 system undergoes a stabilization process with the energy decreasing with time. This stabilization process indicates that the fast cooling procedure employed to obtain the g-100 glass, does not allows the system to reach an optimum thermal equilibrium during quenching. Obviously, thermalization is rapidly reached during the first steps of the slow heating procedures of the nonisothermal devitrification simulations. Figure 7 enable us to determine more exactly the temperature value at which the glasses start to devitrify, and these results inspire us to study the process of devitrification at constant temperature.

The isothermal devitrification was investigated in both g-10 and g-100 systems. Starting from the glasses at 50 K, g-10 and g-100 systems were heated with the same heating rate as before, up to 500 K and 650 K, respectively. At this point these temperatures were kept constant for 200 ps. At this period the system relaxes isothermally. Figure 8 shows the variation of the total energy as a function of time for the isothermal devitrification for both glasses. Two devitrification behaviors are observed: (i) for g-10 the decrease in energy is smooth, and after 115 ps the total energy oscillates around a constant value, indicating the completion of the devitrification; (ii) for g-100, the devitrification is more complex, with four distinct regions on the energy vs time plot. During the initial relaxation process (region 1 in Fig. 8, from $t=0$ to $t\sim110$ ps) the system undergoes a slow decrease on energy. Between $t\sim110$ and $t\sim125$ ps (region 2) a fluctuation over a nearly constant energy is observed. After $t\sim125$ ps the energy abruptly decreases (region 3) to reach, after 155 ps (region 4), a time-constant energy regime due to total crystallization of the system.

In Fig. 9 we show the partial radial distribution functions $g(r)$ obtained during the simulation on the isothermal heat treatment for both glasses. The growing intensity and decrease in the broadening of the peaks, as well as the changes in its position (interatomic distances) reflects the transition from the amorphous to the crystalline phase.

However, the structural evolution during devitrification does not occur in a constant way. In g-10, the $g(r)$ curves presented in Fig. 9 indicates that a large structural organization occurs between 80 and 120 ps and, after this period, little change is observed in the intensity of the peaks. The evolution on $g(r)$ during the devitrification of g-100 follow the same standards, considering the two constant-energy region of Fig. 8 (regions 2 and 4): between 100 and 120 ps of isothermal treatment, a structural evolution is observed, easily visualized on the second and third peaks of Pb-Pb and Pb-F pairs. While no changes are observed between 120 and 140 ps, the devitrification rate increases abruptly between 140 and 160 ps. Finally, as expected, no changes in the peak intensities are observed after 160 ps (region 4 in Fig. 8) where the total energy oscillates around its constant value, and devitrification is expected to reach its completion.

Snapshots of the systems during the isothermal devitrification processes are shown in Figs. 10 and 11. Figures 10(a)–10(f) show the xy-plane view for the system g-100, for various simulation times, while the Figs. 11(a)–11(f)

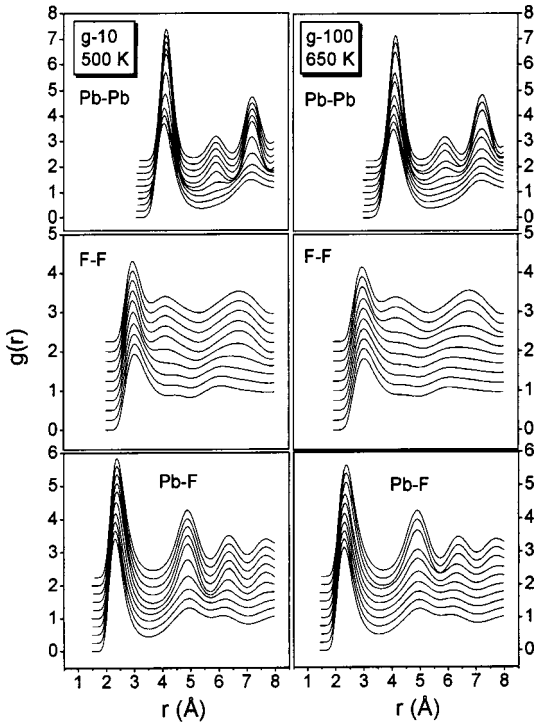

FIG. 9. Pair distribution functions, $g(r)$, during the isothermal heat treatment of both glasses, collected every 20 ps. For each atomic pair, the $g(r)$ curves for the different times where *y*-shifted for a better visualization: from bottom to top: 20, 40, 60, 80, 100, 120, 140, 160, 180, and 200 ps.

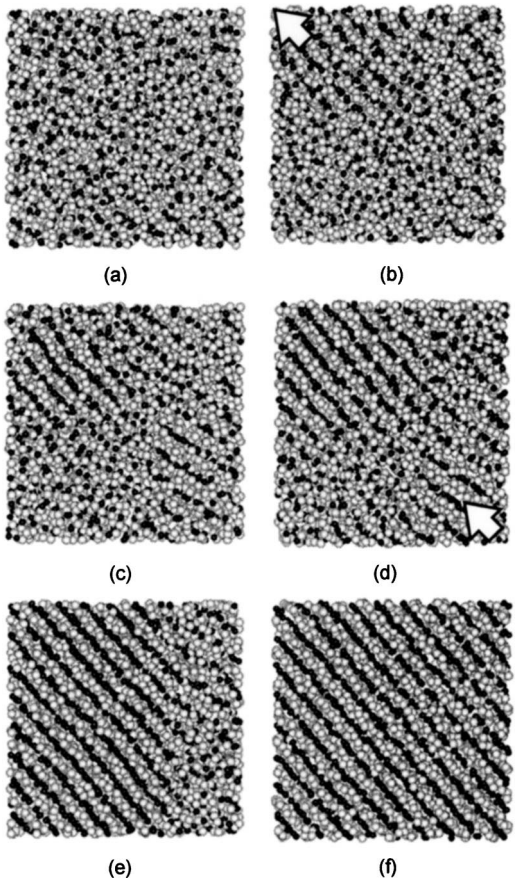

FIG. 10. Snapshots (xy-plane view) of the g-100 system during the isothermal devitrification process at various simulation times: (a) 10 ps, (b) 100 ps, (c) 110 ps, (d) 140 ps, (e) 150 ps and (f) 200 ps. Black spheres: lead atoms; white spheres: fluorine atoms.

reproduce some simulation cells of g-10 system. For the sake of clarity, in Fig. 11 we show only lead atoms, and the cells were rotated by 5° about the y axis. In Figs. 12(a) and 12(b), the simulation cell of g-10 system, after 200 ps at 500 K, is presented in the xy plane view and after a rotation of 5° about the y axis, respectively. Again, only lead atoms are shown for easier visualization.

IV. DISCUSSION

A well-known feature of glasses under a constant (nonisothermal) heating is the dependence of their characteristic temperatures, such as glass transition T_g or devitrification temperatures T_c, with the heating rate. This behavior can be observed, for instance, in differential thermal analysis measurements: high heating rates q will result in larger values for the characteristic temperatures as well as the broadening of the crystallization peak(s). These properties are exploited, for example, in determining the Avrami's exponent n and the activation energy for crystallization, using Johnson-Mehl-Avrami-Kolmogorov (JMAK) expression.[8–11] Our first attempt to reproduce the devitrification processes under heating by molecular dynamics concerns these experimental observations in which larger values for the crystallization temperature of the glass are obtained with faster heating rates.

In this way, various heating procedures ($q_1 = +1$ K/ps, $q_2 = +3$ K/ps, and $q_3 = +5$ K/ps) were performed in g-100 glass, and the plot in Fig. 1 shows clearly the increase of the devitrification temperature of g-100 with the heating rate. Moreover, as the heating procedures employed induce total crystallization of the systems and the crystalline phases obtained are the same (face centered cubic β-PbF_2), whatever the heating rate employed, its energy after crystallization tends to nearly the same values.

Another point to be noted in Fig. 1 concerns the rate of decrease of the energy (stabilization) of the system during devitrification, which depends on the heating rate: faster heating procedures yield a less abrupt change. When the devitrification occurs at constant (nonisothermal) heating rate, the decrease of the internal energy of the system (decrease of the potential energy due to crystallization) is opposed by an increase in the kinetic energy due to the increasing temperature. The result of this competition can be exemplified by Fig. 7, where the steps represent the increasing in the internal energy of the system, due mainly to the increasing in the kinetic energy produced by the rising temperature. When the devitrification temperature T_c is attained, the decrease in the internal energy reflects the changes in the potential energy due to the transition from an amorphous phase (the glass) to a more stable crystalline phase. If a fast heating rate is employed, then the contribution from kinetic energy to the total energy of the system will be larger, due to the fast increase of the temperature. The crystallization range, i.e., the temperature interval in which crystallization occurs, will be, in this case, larger than that obtained with slower-heating procedures. These phenomena are frequently experienced in the laboratory by the differential scanning calorimetry (DSC) or

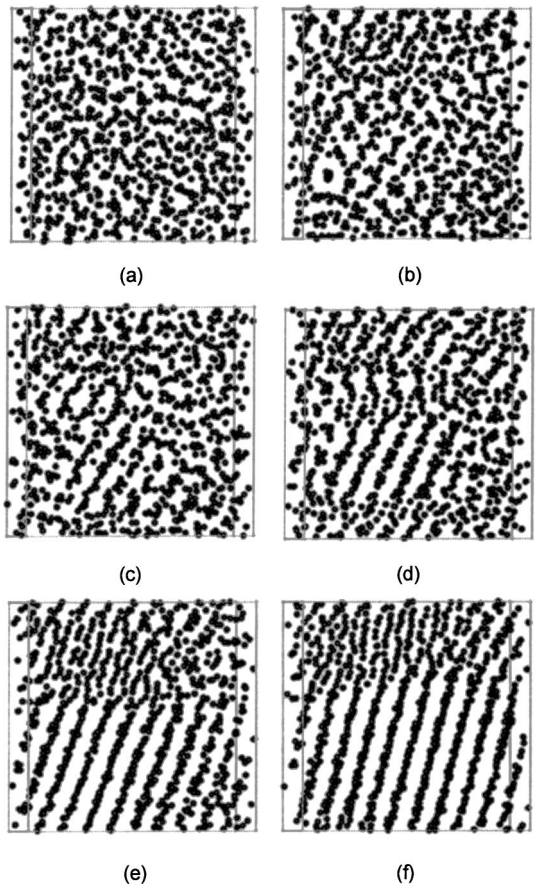

FIG. 11. Snapshots of the g-10 system during the isothermal devitrification process at various simulation times: (a) 10 ps, (b) 110 ps, (c) 140 ps, (d) 160 ps, (e) 180 ps, and (f) 200 ps. The cells were rotate on 5° about the y axis and only lead atoms are shown.

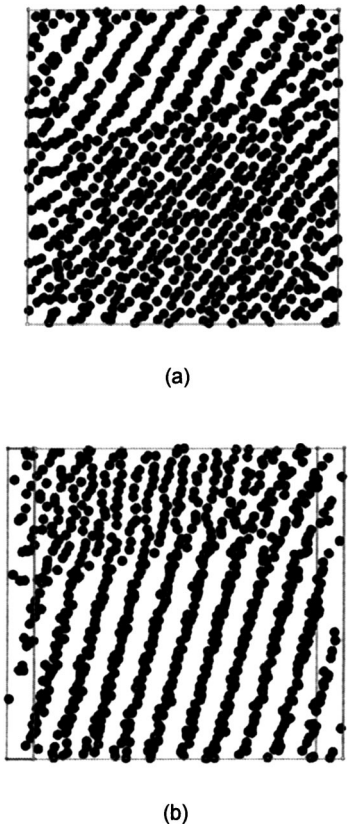

FIG. 12. Simulation cell of the devitrified g-10 system, after 200 ps at 500 K: (a) xy plane view; (b) after rotation of 5° about the y axis. Only lead atoms are shown, for easier visualization.

differential thermal analysis (DTA) exothermic peaks of devitrification: when faster heating rates are employed, lower and broader peaks are obtained, at higher temperatures.

As expected, the rate of cooling from the melt also affects considerably the properties of the resulting glasses. The differences between the glasses obtained at $q_1 = -10$ K/ps and $q_2 = -100$ K/ps studied here are noteworthy. Figure 2 reveals smaller values for the internal energy of glasses obtained at slower-cooling procedures, as the slow-cooling process enables the system to relax and, during the cooling of the supercooled melt, to attain smaller values for its thermodynamic properties, before vitrification. The $g(r)$ curves of the glasses (Fig. 3) indicate that the cooling of the melt at $q_1 = -100$ K/ps produces a glass with completely amorphous Pb-Pb pairs arrangement, while some structuring is observed on the Pb-F and F-F pairs. For the g-10 glass, this organization is more apparent for Pb-F and F-F pairs and, moreover, some degree of organization is also observed on the cationic network, at about 7.5 Å. This led us to conclude that the high mobility of the fluorine ions (related to the relatively weak Pb-F interactions[12] in β-PbF_2) favors some degree of organization of the anionic network during the cooling processes, at -10 and -100 K/ps, while a weak organization on the cationic network (the lead atoms being far less mobile) is observed using slower cooling rates only, i.e., -10 K/ps. Moreover, as these structural stabilization processes are more pronounced in g-10 glass, it is expected that it possesses smaller values of internal energy than g-100.

Another important point revealed by this study on the influences of the cooling rate on glass formation is the glass transition temperature value. The plot of $g_{\min}(r)/g_{\max}(r)$ versus temperature, shown in Fig. 2, indicates the T_g value on the intercept of the slopes at high (liquid) and low (glass) temperature regimes. The results obtained for g-10 and g-100 are perfectly in accord with the expected behavior, with g-10 presenting a smaller value of T_g than g-100.

Results obtained from the nonisothermal heating of the glasses indicate that the devitrification temperatures obtained for the glasses are in good agreement with the T_g values obtained. During the heating of a glass it is expected that it will crystallize at a temperature above T_g, due to the viscous flow allowing the atomic mobility and, in fact, our results reveal the devitrification of g-10 and g-100 starting respectively at 500 and 650 K, 20 K above the T_g values obtained, 480 K and 630 K on g-10 and g-100, respectively. The $g(r)$ analysis of the nonisothermal devitrification process (Fig. 5) reveals that the structural evolution of both glasses are identical, but not intense. The weak intensity of the peaks in Fig. 5, mainly those related to the pairs involving fluorine, reflects the high mobility of the anions. The atomic mobility can be evaluated by the approximate diffusion coefficients D as shown in Fig. 6. The peaks observed on the D_{Pb} curves, with maxima at 600 K for g-10 and 700 K for g-100 glasses, are related to the increase in the cationic mobility at tempera-

tures above T_g, which allows the system to devitrify. After the accomplishment of the devitrification, the diffusive movements of the lead atoms decreases rapidly, as they are restricted to the regular fcc lattice sites of the crystalline PbF_2. On the other hand, the diffusion coefficient of fluorine atoms, weakly attached to the cationic network,[12] exhibit a monotonic rise with temperature as one would expect. As a consequence, F-F partial $g(r)$ shows little structural evolution after devitrification, while Pb-Pb and Pb-F display stronger structural evolution (see Fig. 5).

A comparison between the diffusion coefficients of lead and fluorine atoms in vitrified and crystalline PbF_2, reveals that the amorphous character of the glassy matrix affects considerably the mobility of the fluorine atoms. The superionic properties of this and others systems with fluorite-type structures have been related to the generation of Frenkel defects, activated by the rising temperature, and the superionic transition is also called ''sublattice melting,'' (Ref. 12) due to the high anionic mobility, comparable to those found in liquids. The results presented here indicate that the presence of defects in the glassy network (such as voids) favors the activation of the processes related to the anionic mobility on the glasses.

The nonisothermal devitrification performed gave us important information such as the temperature of beginning of crystallization, qualitative insight on the degree of devitrification, the occurrence of stabilization processes, etc. However, in the nonisothermal procedure adopted, the devitrification processes occur in a relatively large region of temperature (reaching 150 K in g-10!). Moreover, as discussed above, the rising temperature does not allows the anionic network to organize efficiently during the nonisothermal devitrification, due to the high mobility of the fluorine atoms.

On the other hand, with the isothermal devitrification procedures, as temperature is maintained constant in relatively low values, more pronounced peaks in $g(r)$ are observed when comparing Figs. 5 and 9. An analysis on Figs. 8 and 9 indicates that the time period in which energy decreases is related to a fast crystal growth regime. For g-100, the energy versus time plot in Fig. 8 indicates the occurrence of two decreasing-energy and two constant-energy regimes (regions 1, 3, 2, and 4, respectively). From $g(r)$ in Fig. 9 we were able to identify the two periods of fast crystal growth, between 100 and 120 ps and between 140 and 160 ps.

The snapshots presented in Figs. 10–12 also evidence the differences in the devitrification features between g-10 and g-100. The structural organizations occurring during the isothermal treatments are clearly observed. The atomic positions, initially disposed randomly in the glassy matrix, present a gradual organization process, until complete crystallization is achieved. In g-100, the formation of a single crystal (limited by the cell dimensions) is observed, and the devitrification starts, as illustrated in Fig. 10, in the upper left quadrant on the xy plane. Crystallization progresses with the crystal growing in the direction of the arrow [Fig. 10(b)]. However, limitations imposed by the periodic boundary conditions and the size of the system ($L=35.58$ Å), promote an interesting effect in the crystal growth process. When the growing crystalline phase crosses the upper left size of the simulation box, image atoms from this phase, due to the periodic boundary conditions, immediately appear in the lower right side of the simulation box [Fig. 10(d)]. Between the crystalline phases, lies an amorphous phase which, probably strongly ''compressed'' between the stationary (upper left side of the simulation box) and the growing (lower right side) crystalline phases, seems to difficult the progression of the crystalline growth. This purely mathematical effect, is a possible explanation to the constant-energy period and slow crystal growth observed between 110 and 130 ps of isothermal treatment in g-100 (Figs. 8 and 9).

The occurrence of more than one crystalline plane in g-10 match perfectly with the experimental behavior of glasses obtained from different cooling rates. In our studies, the occurrence of a single crystal during devitrification of g-100 reveals the lack of propitious regions to the crystallization (or crystallization nuclei). This can be related to the fast-cooling rate employed, but one must keep in mind that the relatively small number of particles can also contribute to the difficulty of forming more than one crystal. On the other hand, the slow decrease in temperature, employed during the production of g-10, allows the relaxation and organization of various regions on the bulk glass, giving origin to various crystallization nuclei, which one observes in the development of two crystalline planes in the devitrified g-10, clearly visualized with rotations performed on the simulation cell, reproduced in Fig. 11.

V. CONCLUSIONS

The vitrification and devitrification features were investigated by means of molecular dynamic simulations. First, the consequences of the heating rate on the devitrification temperature were identified, where an increase in the temperature of the beginning of devitrification was observed, as well as a slower devitrification process, when faster heating rates were employed. These features are well known to glass researchers: when differential thermal analysis measurements (DSC or DTA) are performed with higher-heating rates, broader and less intense devitrification peaks, dislocated to higher temperature values are observed. Molecular dynamics simulations were also used to study another well-known experimental observation: the dependence of the glass properties on its thermal history, in our case the cooling rate employed. Two glasses were obtained with quenching rates $q_1=-10$ K/ps and $q_2=-100$ K/ps (labeled g-10 and g-100, respectively). Diffusion coefficients analysis during glass and crystal heating, indicates that the presence of defects in the glassy matrix favors the transition processes from the ionic to a superionic state, with high mobility of fluorine atoms, responsible for the high anionic conduction of lead fluoride. Moreover, it was observed the increase on the mobility of lead atoms at temperatures above T_g leading to devitrification, been possible to relate the temperature of maximum diffusive Pb rate, i.e., the peaks on D_{Pb} versus temperature plot (Fig. 6), as the temperature of maximum crystal growth rate. In other words, the devitrification of a PbF_2 glass is governed by the lead atoms diffusive movements when the viscosity decreases at temperatures above

T_g. As expected, these two glasses presented different devitrification features. The glass g-10 presents smaller T_g and T_c values than g-100 and, after isothermal heat treatment, it devitrifies in two crystalline grains, while g-100 produces one single crystal. During the cooling from the melt, a more pronounced structural organization was observed using the slower procedure, giving origin to g-10. The relaxation processes during vitrification (obviously more efficient on the slow cooling process) imply that regions in the glass bulk are more susceptible to devitrification, which is reflected in the origin of two crystalline grains in g-10. The hypothesis of the occurrence of relaxation processes is also supported by the higher degree of organization observed on the $g(r)$ curves and the smaller values of energy for the glass g-10 (Figs. 3 and 2, respectively). Comparison of the nonisothermal and isothermal devitrification processes, enables us to identify the reasons for the weak intensity of the $g(r)$ peaks, mainly those related to the Pb-F and F-F pairs, after the nonisothermal devitrification: at high temperatures, fluorine atoms display high values of diffusion coefficients, which reflects a larger distribution of sites for this anion and, consequently, broader peaks on $g(r)$ at higher temperatures. Finally, the devitrification temperatures of both glasses (T_c =500 and 650 K in g-10 and g-100, respectively) are reasonable according to the glass transition temperatures obtained from the simulations (T_g=480 and 630 K in g-10 and g-100, respectively), T_g occurring at 20 K below T_c in both cases.

ACKNOWLEDGMENTS

Thanks are due to Dr. Marcel Poulain for valuable discussions. This work was supported by FAPESP (Brazil).

[1] A. Karthikeyan and K. J. Rao, J. Phys. Chem. B **101**, 3105 (1997).
[2] For a review see S. Chaussedent, V. Teboul, and A. Monteil, Curr. Opin. Solid State Mater. Sci. **7**, 111 (2003).
[3] T. Nanba, T. Miyaji, J. Takada, A. Osaka, Y. Miura, and I. Yasui, J. Non-Cryst. Solids **117**, 131 (1994).
[4] M. A. P. Silva, A. Monteil, Y. Messaddeq, and S. J. L. Ribeiro, J. Chem. Phys. **117**, 11, 5366 (2002).
[5] A. B. Walker, M. Dixon, and M. J. Gillan, J. Phys. C **15**, 4061 (1982).
[6] J. E. Enderby and A. C. Barnes, Rep. Prog. Phys. **53**, 85 (1990).
[7] G. Tammann, *Der Glaszustand* (Leopold Voss Verlag, Leipzig, 1933).
[8] J. W. Christian, *The Theory of Phase Transformations in Metals and Alloys: Part I*, 2nd ed. (Pergamon, New York, 1975).
[9] W. A. Johnson and R. F. Mehl, Trans. AIME **135**, 416 (1939).
[10] A. E. Kolmogorov, Akad. Nauk SSR. ISV. Ser. Mat. **1**, 355 (1937).
[11] M. Avrami, J. Chem. Phys. **8**, 212 (1940).
[12] I. Kosaki, Appl. Phys. A: Solids Surf. **49**, 413 (1989).